Korean J. Chem. Eng., 33(6), 1781-1787 (2016)
DOI: 10.1007/s11814-016-0050-5

pISSN: 0256-1115
eISSN: 1975-7220

Preferential CO oxidation over supported Pt catalysts

Kyung-Won Jeon*, Dae-Woon Jeong*, Won-Jun Jang*, Jae-Oh Shim*, Hyun-Suk Na*, Hak-Min Kim*, Yeol-Lim Lee*, Byong-Hun Jeon, Seong-Heon Kim*, Jong Wook Bae***, and Hyun-Seog Roh*,†**

*Department of Environmental Engineering, Yonsei University, 1 Yonseidae-gil, Wonju, Gangwon-do 26493, Korea
**Department of Natural Resources and Environmental Engineering, Hanyang University, 222 Wangsimni-ro, Seongdong-gu, Seoul 04763, Korea
***School of Chemical Engineering, Sungkyunkwan University (SKKU), 2066 Seobu-ro, Suwon, Gyeonggi-do 16419, Korea
(*Received 15 September 2015 • accepted 18 February 2016*)

Abstract−Preferential CO oxidation reaction has been carried out at a gas hourly space velocity of 46,129 h^{-1} over supported Pt catalysts prepared by an incipient wetness impregnation method. Al_2O_3, MgO-Al_2O_3 (MgO=30 wt% and 70 wt%) and MgO were employed as supports for the target reaction. 1 wt% Pt/Al_2O_3 catalyst exhibited very high performance (X_{CO}>90% at 175 °C for 100 h) in the reformate gases containing CO_2 under severe conditions. This result is mainly due to the highest Pt dispersion, easier reducibility of PtO_x, and easier electron transfer of metallic Pt. In addition, 1 wt% Pt/Al_2O_3 catalyst was also tested in the reformate gases with both CO_2 and H_2O to evaluate under realistic condition.

Keywords: Preferential CO Oxidation, Pt/Al_2O_3, Dispersion, Reducibility, Electron Transfer

INTRODUCTION

Fuel cells have been major candidates for an efficient alternative energy source to fossil fuels. Proton exchange membrane fuel cells (PEMFCs) using H_2 are an especially promising source of portable power for transportation and residential systems [1,2]. H_2 can be produced on-board by steam reforming of methane (SRM) or partial oxidation of methane (POM) followed by a water gas shift reaction (WGS) [3-5]. However, H_2 produced from hydrocarbons is usually mixed with a trace amount of CO, which strongly poisons PEMFCs electrodes [6,7]. Therefore, CO should be reduced to an acceptable level before reaching the PEMFCs. Several approaches have been applied to remove CO in reformate gas: pressure swing adsorption (PSA), CO methanation, and preferential CO oxidation (PROX). The PSA is not suitable for small-scale fuel processor, due to the large dimensions and the high costs of the compressor [8]. In addition, CO methanation has disadvantages for the loss of H_2 by the intended reaction of CO with H_2 (CO methanation) and the undesired side reaction of coexisting CO_2 with H_2 (CO_2 methanation) [9]. Therefore, PROX has been accepted as one of the most encouraging among the methods proposed to remove residual CO [10].

In the last few years, novel catalyst compositions have been intensively investigated to develop highly active catalysts. Gold [11-14], platinum group metals (Pt, Pd, Ru, and Rh) [15-19], and transition metal-based catalysts [20-22] have been studied. Supported Pt catalysts have received much interest because of their high activity and remarkable selectivity for PROX [23,24].

†To whom correspondence should be addressed.
E-mail: hsroh@yonsei.ac.kr

PROX activity is reported to depend on a number of factors, including the preparation method, the nature of the support, testing conditions, and reactor design [25-36]. Souza et al. reported that catalytic activity depends strongly on the nature of the support [32]. Recently, various supports have been intensively studied to find the optimized supports. As one of the most common supports, Al_2O_3 would be preferable support for Pt catalysts as compared with other metal oxides because of its cheapness, high surface area, high thermal stability, and well controllable porosity [33-35]. In addition, Uysal reported that MgO supported Pt catalysts have also been investigated to improve PROX activity since MgO stabilizes the metals in unusual oxidation states and prevents sintering of metal atoms [36]. Hao et al. also reported that MgO supported on gold absorbed CO_2 and formed carbonate and bicarbonate, which results in changes in catalyst behavior in CO oxidation [37]. Some researchers have studied MgO additive on alumina supported metal catalyst, which may lead to lowering of the reaction barrier of O_2 adsorption [38]. Although some comparative studies of supported Pt catalysts have been reported [15,19,23,24,26], the comparative study on physicochemical characteristics of the Al_2O_3, MgO, and MgO-Al_2O_3 supports on the PROX activity has not been investigated in detail over Pt catalysts.

The testing conditions strongly affect catalytic performance [27,28]. For example, the presence of CO_2 in the reactant feed decreases PROX activity [22]. The negative effect of CO_2 on catalytic performance is related to the competitive adsorption of CO and CO_2 on the catalyst surface. Several authors have proposed enhancing the CO oxidation rate in the presence of H_2O [23,28]. H_2O helps to create only PtO_x species, which may increase the number of hydroxyl groups available at the surface for PROX. However, most of the previous work has been conducted on mixtures comprising only CO and H_2 and under artificial conditions. Therefore, the inhibi-

tion of PROX over supported Pt catalysts by CO_2 has been investigated [39].

Mariño et al. [21] proposed that decreased PROX activity with increasing CO_2 in the stream (up to 15%) could be related to competitive adsorption of CO_2 on the active sites, inhibition of oxygen mobility upon carbonate formation on the support, or both. Gamarra and Martinez-Arias [40] addressed the ability of CO_2 to hinder interfacial redox activity by forming carbonate-type species. Thus, the presence of CO_2 without H_2O makes the conditions more severe. Therefore, the supported Pt catalyst should be evaluated under realistic conditions, which require high resistance to inhibition by CO_2.

To develop supported Pt catalysts that are highly active in realistic conditions, we compared PROX activity and selectivity over Pt catalysts supported on Al_2O_3, MgO-Al_2O_3 (MgO=30 wt% and 70 wt%), and MgO and tried to explain the differences in catalytic activity with various characterization methods. Consequently, the goal of this work was to develop highly active and stable catalyst to get maximum CO conversion and high CO_2 selectivity in PROX under severe conditions.

EXPERIMENTAL

1. Catalyst Preparation

Al_2O_3 (99%, SASOL), MgO-Al_2O_3 (MgO loading=30 wt% and 70 wt%, SASOL), and MgO were employed as supports. MgO was prepared by pre-calcination reported earlier [41]. Pt (Pt loading of 1 wt%) was loaded by an incipient wetness impregnation method. $Pt(NH_3)_4(NO_3)_2$ (99%, Aldrich) was used as a precursor. The catalysts were calcined at 500 °C for 6 h.

2. Characterization

The surface areas of the prepared catalysts were determined using N_2 (BET) adsorption at −196 °C by commercial equipment, the ASAP 2010 (Micromeritics). X-ray diffraction (XRD) was performed using a Rigaku D/MAX-IIIC diffractometer with nickel-filtered Cu-Kα radiation (40 kV tube voltage and 50 mA tube current). CO-chemisorption was measured using an Autochem 2920 (Micromeritics). The detailed procedure for CO-chemisorption was described earlier [41]. The amount CO chemisorbed was calculated by assuming an adsorption stoichiometry of one CO per Pt surface atom ($CO/Pt_{surface}=1$) to estimate Pt dispersion and crystallite size. H_2 temperature-programmed reduction (TPR) was performed on a BEL-CAT (BEL JAPAN INC.). The catalyst (100 mg) was pre-treated at 250 °C for 1 h under Ar flow (50 ml/min) and then cooled to room temperature. The catalyst was re-heated with a ramping rate of 10 °C/min and a flow rate of 50 ml/min up to 520 °C under 10% H_2 in Ar gas. The sensitivity of the detector was calibrated by reducing a known weight of NiO [42,43]. XPS spectra were obtained using a Kα spectrophotometer (Thermo-Scientific), with a high-resolution monochromator. The pressure of the analysis chamber was maintained at 6.8×10^{-9} mbar and with the detector in constant energy mode with a pass energy of 100 eV for the survey spectrum and 50 eV for the detailed scan. The binding energy was calibrated using the C 1s transition, which appeared at 284.6 eV [44].

3. Catalyst Activity

The prepared catalyst (59 mg) was charged in a micro-tubular quartz reactor (I.D.=4 mm). Preferential CO oxidation was carried out by increasing the temperature from 100 to 175 °C under atmospheric pressure. Before the reaction, the catalyst was reduced at 400 °C for 1 h under a mixture of 5% H_2/N_2. The simulated reformate gas consisted of 0.80 vol% CO, 62.65 vol% H_2, 16.76 vol% CO_2, 0.99 vol% CH_4, 18.80 vol% N_2, which represents a typical reformed gas from WGS. The feed $[O_2]/[CO]$ ratio was intentionally fixed at 1.0. A GHSV of 46,129 h^{-1} was used to screen the catalysts. The effect of H_2O addition on catalytic activity was investigated at $H_2O/(CH_4+CO+CO_2)=1$. The effluent was passed through a chiller (JS Research) and moisture trap with absorbent (Drierite) to condense residual water, and then was analyzed with an on-line micro gas chromatograph (Agilent 3000) equipped with a TCD detector. A micro-GC with a molecular sieve and plot U columns were used. The CO conversion and CO_2 selectivity were calculated using the following formulas.

$$\text{CO conversion (\%)}=([CO]_{in}-[CO]_{out})/[CO]_{in}\times100 \quad (1)$$

$$CO_2\text{ selectivity (\%)}=([CO]_{in}-[CO]_{out})/\{2\times([O_2]_{in}-[O_2]_{out})\}\times100 \quad (2)$$

Turnover frequency (TOF) was calculated using the following equation.

$$TOF\ (s^{-1})=\{([CO]_{in}-[CO]_{out})\times AB_M\times F\}/(D\times W\times X_M) \quad (3)$$

where $[CO]_{in}$ and $[CO]_{out}$ are the inlet and outlet concentrations of CO, AB_M is the atomic weight of metal M, F is the total flow rate (mol s^{-1}), D is the metal dispersion, W is the mass of catalyst (g), and X_M the metal content (g_{metal}/g_{cat}), respectively.

RESULTS AND DISCUSSION

1. Catalyst Characterization

Table 1 summarizes the characteristics of supported Pt catalysts. Pt/Al_2O_3 showed the highest BET surface area (156 m^2/g) among the supported Pt catalysts. On the contrary, Pt/MgO showed the lowest BET surface area (41 m^2/g). The BET surface area decreased in the following order: Pt/Al_2O_3>Pt/MG30>Pt/MG70>Pt/MgO.

XRD patterns of supported Pt catalysts are shown in Fig. 1. For all the catalysts, reflections corresponding to Pt metal particles could not be detected because of a low Pt loading content (≤1 wt%). The XRD patterns of Pt/MgO-Al_2O_3 catalysts are similar to that of Pt/Al_2O_3 but shifted to lower angles with increasing MgO content in a support. This indicates that Al^{3+} is partially substituted with Mg^{2+} in Pt/MgO-Al_2O_3 [45]. Therefore, it can be said that a solid solu-

Table 1. Characteristics of supported Pt catalysts

Catalysts	Catalyst S.A.[a] (m^2/g)	Support S.A.[a] (m^2/g)	Crystallite size of support[b] (nm)
Pt/Al_2O_3	156	162	5.8
Pt/MG30	143	148	N.A.[c]
Pt/MG70	120	166	4.9
Pt/MgO	41	63	30.4

[a]Estimated from N_2 adsorption at −196 °C

[b]Estimated from XRD

[c]Not available due to very broad and weak XRD peaks

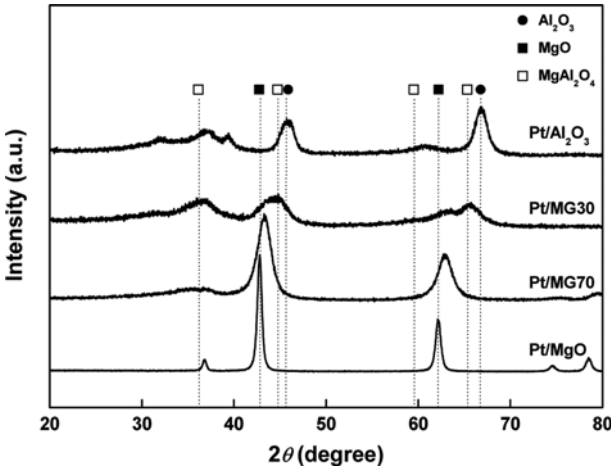

Fig. 1. XRD patterns of supported Pt catalysts.

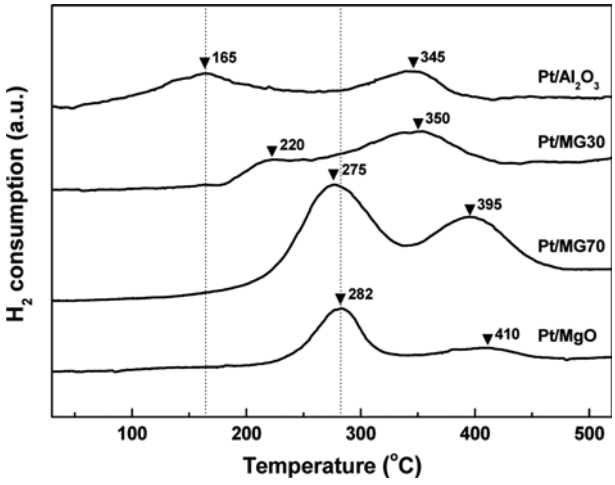

Fig. 2. TPR patterns of supported Pt catalysts.

Table 2. CO-chemisorption and TOF (175 °C) results of supported Pt catalysts

Catalysts	Pt dispersion (%)	Pt S.A. (m^2/g)	Pt crystallite size (nm)	TOF (s^{-1})
Pt/Al_2O_3	88.7	2.19	1.06	0.090
Pt/MG30	51.5	1.27	1.83	0.089
Pt/MG70	39.0	0.96	2.42	0.091
Pt/MgO	24.8	0.61	3.80	0.110

tion is formed for MgO-Al_2O_3. The crystallite sizes (Table 1) of the supports were calculated by using Scherrer's equation. The crystallite size of MG30 could not be calculated due to very broad and weak peaks. The crystallite sizes of MG70 and Al_2O_3 were 4.9 and 5.8 nm, respectively. Pure MgO had the largest crystallite size, 30.4 nm.

Table 2 summarizes CO-chemisorption results. Pt dispersion of Pt/Al_2O_3 was the highest among the prepared catalysts, while Pt dispersion of Pt/MgO was the lowest. Pt dispersion decreased in the following order: Pt/Al_2O_3 (88.7%)>Pt/MG30 (51.5%)>Pt/MG70 (39.0%)>Pt/MgO (24.8%). Thus, Pt/Al_2O_3 had the smallest Pt crystallite size, and Pt/MgO had the largest. It has been reported that higher Pt dispersion and smaller Pt crystallite size result from higher BET surface area, which is helpful to enhance catalytic activity due to more surface active sites exposed to reactants [46,47]. Therefore, the Pt/Al_2O_3 catalyst was expected to have a higher CO conversion than other catalysts for PROX.

TPR patterns of supported Pt catalysts are depicted in Fig. 2. The TPR patterns of supported Pt catalysts were characterized by lower and medium temperature peaks located at ca. 200 and ca. 400 °C, respectively. Lower temperature peaks can be attributed to the reduction of surface PtO_x species, while higher temperature peaks can be assigned to the reduction peak of PtO_x species, which has an interaction with support [5]. For the Pt/Al_2O_3, two reduction peaks can be seen 165 and 345 °C. The first low temperature peak of Pt/Al_2O_3 can be assigned to the reduction of surface PtO_x species. The last peak at 345 °C is due to the reduction of PtO_x species, which interact with Al_2O_3 [40]. For Pt/MG30 and Pt/MG70 catalysts, the first peak appears at 220 and 275 °C, respectively, and the second reduction peak is present at 350 and 395 °C, respectively. The first peak is due to the reduction of surface PtO_x species. The second peak is possibly assigned to the reduction of PtO_x species, which interact with the support. In the case of Pt/MgO, the first peak shows at 282 °C and the second peak at 410 °C. Note that the first reduction peaks of Pt/MG30, Pt/MG70 and Pt/MgO catalyst are shifted to higher temperature than that of Pt/Al_2O_3 catalyst. Clearly, it is confirmed that the Pt/Al_2O_3 catalyst can be reduced at the lowest temperature. This result indicates that the Pt/Al_2O_3 catalyst has easier reducibility of PtO_x species. It is known that easier reducibility of PtO_x species leads to greater number of active sites participating in the reaction [46]. It can be concluded that the easier reducibility of catalysts may strongly affect catalytic activity for the PROX [32,46,48,49]. As a consequence, the Pt/Al_2O_3 catalyst in this study is expected to have a higher CO conversion than others for PROX under severe conditions.

To identify the reducibility of supported Pt catalysts, XPS analysis was carried out. The XPS survey scan of supported Pt catalysts is presented in Fig. 3(a). The XPS spectra, located from 60 to 340 eV, contain Pt 4f, Pt 4d, Al 2p, Al 2s, Mg 2s, Mg KLL, and C 1s peaks. For the Pt/MG30, Pt/MG70, and Pt/MgO catalyst, the photoelectron peaks assigned to Pt 4d are buried due to the low Pt loading. Thus, Pt 4d peaks could not be distinguished. In addition, the Pt 4d peaks intrinsically decrease the precision of the measurements due to very broad and weak peaks compared to Pt 4f peaks [50]. Therefore, the Pt 4f peaks are considered to confirm the redox properties of supported Pt catalysts. Although Pt 4f peaks are located in similar positions to Al 2p peak, Pt $4f_{5/2}$ binding energy of metallic Pt, the active species in PROX, can be detected because the Pt $4f_{5/2}$ binding energy of metallic Pt is the same as Al 2p [50,51]. Thus, metallic Pt of Pt $4f_{5/2}$ photoelectron peaks were detected as shown in Fig. 3(b). The binding energy of metallic Pt shifted in the following order: Pt/Al_2O_3 (73.46 eV)<Pt/MG30 (74.19 eV)< Pt/MG70 (74.31 eV)<Pt/MgO (74.37 eV). On the basis of the observed shift in binding energy of metallic Pt, the electrons were transferred from supports to metallic Pt to degrees in the following order: Pt/Al_2O_3>Pt/MG30>Pt/MG70>Pt/MgO [52]. This result demonstrates that electron transfer to metallic Pt in Pt/Al_2O_3 may

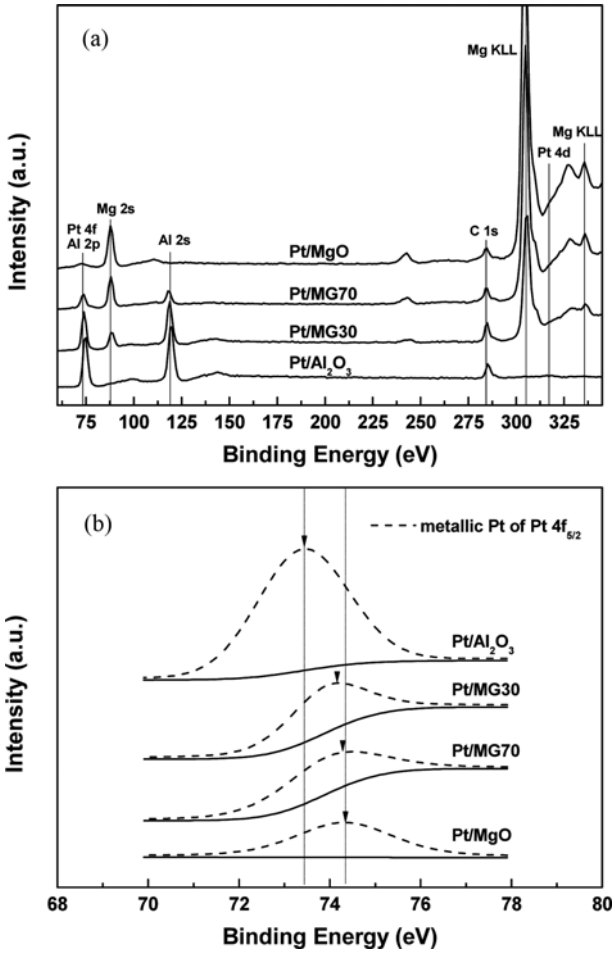

Fig. 3. XPS spectra of supported Pt catalysts: (a) Survey scan of supported Pt catalysts, (b) enlarged figure for metallic Pt of Pt $4f_{5/2}$.

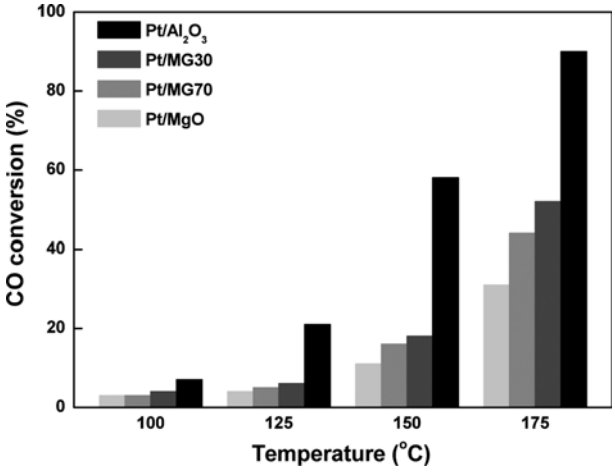

Fig. 4. CO conversion with reaction temperature over supported Pt catalysts (Reaction condition: $[O_2]/[CO]=1.0$; GHSV=46,129 h^{-1}).

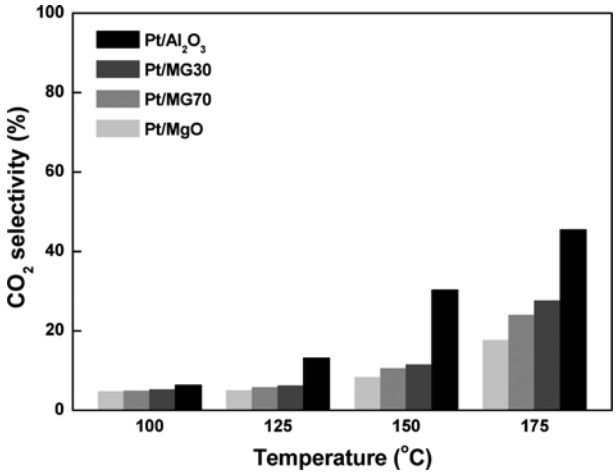

Fig. 5. CO_2 selectivity with reaction temperature over supported Pt catalysts (Reaction condition: $[O_2]/[CO]=1.0$; GHSV=46,129 h^{-1}).

be easier than the other catalysts. In addition, the binding energy of metallic Pt of Pt/Al_2O_3 (73.46 eV) is lower than that of Pt foil (74.0 eV) [52]. The lower binding energy of metallic Pt in Pt/Al_2O_3 catalyst indicates that this metallic Pt was in a negative oxidation state, $Pt^{\delta-}$ [53]. It is reported that easier electron transfer of metallic Pt leads to the reduction of PtO_x species at a lower temperature [53]. Therefore, as shown in TPR patterns, the PtO_x species of Pt/Al_2O_3 catalyst can be reduced at the lowest temperature.

2. Reaction Results

To develop highly active catalyst under severe condition, activity tests were carried out in PROX using the typical reformate gas without H_2O. Fig. 4 illustrates CO conversion results over supported Pt catalysts. Pt/Al_2O_3 had the highest CO conversion at reaction temperatures from 100 to 175 °C. At 100 °C, all the catalysts showed low CO conversion. The highest CO conversion by Pt/Al_2O_3 (21%) occurred at 125 °C. The other catalysts showed negligible CO conversion at the same temperature. At a reaction temperature of 150 °C, CO conversion by the Pt/Al_2O_3 catalyst was three-times higher than that of the other catalysts. The highest CO conversion by Pt/Al_2O_3 occurred at 175 °C. At this temperature, the CO conversion was ranked as follows: Pt/Al_2O_3 (90%)>Pt/MG30 (52%)>Pt/MG70 (44%)>Pt/MgO (31%). Pt/Al_2O_3 catalyst can be a promising catalyst for PEMFCs. Due to the loss of heat energy for cooling H_2-rich gas, operation at a higher temperature, e.g., at the temperature level of preceding water gas shift step in a reformer of about 200 °C, may be more attractive [54]. The TOF results are provided in Table 2. The TOF of CO conversion took into account the results of the CO-chemisorption experiments. At a reaction temperature of 175 °C, TOF are 0.090 s^{-1} for Pt/Al_2O_3, 0.089 s^{-1} for Pt/MG30, 0.091 s^{-1} for Pt/MG70, and 0.110 s^{-1} for Pt/MgO. Although Pt/MgO catalyst has the highest TOF value among the prepared catalysts, Pt/MgO catalyst showed the lowest PROX activity due to its reduction property and the lowest Pt dispersion.

Fig. 5 depicts CO_2 selectivity over supported Pt catalysts. CO_2 selectivity of supported Pt catalysts is less than 50%. For all the prepared catalysts, no O_2 is detected in the exit stream of the reactor. As a result, 100% conversion of O_2 is obtained within the reaction temperature range for all catalysts. Complete O_2 conversion in excess

Table 3. Comparative data on CO conversion and CO_2 selectivity over Pt/Al_2O_3 catalysts for PROX (T=175 °C)

Catalysts	GHSV (h^{-1})	$[O_2]/[CO]$	X_{CO}	S_{CO_2}	Reference
1 wt% Pt/Al_2O_3	46,129	1	90%	45%	Present work
1 wt% Pt/Al_2O_3	12,000	1	82%	41%	Zhang et al. [55]
0.5 wt% Pt/Al_2O_3	28,000	1	75%	45%	Gómez et al. [56]
1 wt% Pt/γ-Al_2O_3	60,000	2	100%	24%	Koo et al. [46]

O_2 conditions leads to limitations on CO_2 selectivity (S_{CO_2}≤50%). For Pt/Al_2O_3, the trend of CO_2 selectivity is similar to that of CO conversion. As a result, Pt/Al_2O_3 catalyst exhibited the highest CO_2 selectivity of the prepared catalysts. The CO_2 selectivity of a Pt catalyst supported with MgO is lower than that of Pt/Al_2O_3. The CO_2 selectivity decreased with MgO use in the support. This result can be explained by the basic nature of MgO, which gives rise to a strong interaction with CO_2 [23]. As a result, the CO_2 selectivity of the Pt/Al_2O_3 catalyst is the highest of the catalysts tested in this study, even in the presence of CO_2. Table 3 provides a comparison of reported data on CO conversion and CO_2 selectivity at 175 °C for the PROX using Pt/Al_2O_3 catalysts [46,55,56]. Clearly, the catalyst prepared in this study shows higher activity and selectivity in PROX than the catalysts reported by Zhang et al. and Gómez et al. Koo et al. reported that CO conversion of 1 wt% Pt/γ-Al_2O_3 prepared by impregnation is higher in this study at the same temperature, while CO_2 selectivity is lower. The differences of catalytic performance are mainly caused by higher $[O_2]/[CO]$ ratio. CO oxidation rate and undesirable H_2 oxidation rate increase with increasing $[O_2]/[CO]$ ratio, which results in higher CO conversion and lower CO_2 selectivity. In addition, PROX in this study is carried out under realistic condition, typical reformate feed gas from WGS containing CO_2.

The excellent catalytic performance of the Pt/Al_2O_3 catalyst in PROX can be explained as follows. First, the reduction property is an important factor. Ratnasamy et al. [57] reported that catalytic performance depends strongly on the reduction properties of the catalyst in PROX. According to the TPR results, reduction of a Pt/Al_2O_3 catalyst is possible at 165 °C, which is the lowest reduction temperature. This indicates that Pt/Al_2O_3 catalyst has easier reducibility of PtO_x species than other catalysts. In heterogeneous catalysis, two possible mechanisms have been proposed, Langmuir-Hinshelwood mechanism and Rideal-Eley mechanism, as shown in Scheme 1. In the Langmuir-Hinshelwood mechanism, two reacting molecules are adsorbed on neighboring sites before the reaction takes place, whereas in the Rideal-Eley mechanism, only one of the molecules is adsorbed and the other one reacts directly from the gas phase, without adsorbing. In PROX, CO oxidation follows a Langmuir-Hinshelwood mechanism, where O_2 and CO compete in the adsorption on the same type of active sites [58,59]. The easier reducibility of PtO_x accelerates production of the CO adsorbed over metallic Pt, favoring the oxygen adsorption and CO_2 production. As a result, the easier reducibility of Pt/Al_2O_3 catalyst most likely results in it having the highest CO conversion and CO_2 selectivity. Second, the Pt dispersion also has a significant effect on the catalytic performance. The catalytic activity of supported Pt catalysts and Pt dispersion had the same trend. Therefore, the Pt/Al_2O_3 catalyst, which had the highest Pt dispersion (88.7%) and the smallest Pt crystallite size (1.06 nm), showed remarkable catalytic performance.

Fig. 6 illustrates stability of Pt/Al_2O_3 catalyst. To check the stability of Pt/Al_2O_3 catalyst in PROX, CO conversion data were collected at 175 °C and at a GHSV of 46,129 h^{-1} for 100 h. Huang et al. [60] reported that CO conversion (initial X_{CO}=70%) rapidly decreased to 40% in the presence of CO_2 over an Ir/CeO_2 catalyst at a GHSV of 40,000 h^{-1}. The Pt/Al_2O_3 catalyst in this study showed CO conversion of more than 90% for up to 100 h without detectable deactivation. To the best of our knowledge, it is rare for supported Pt catalysts to have high activity and stability at a GHSV of 46,129 h^{-1} in PROX.

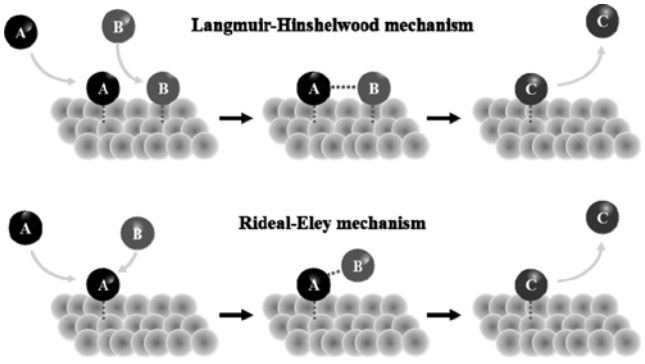

Scheme 1. Schematic presentation of molecular mechanisms for heterogeneous catalytic reaction.

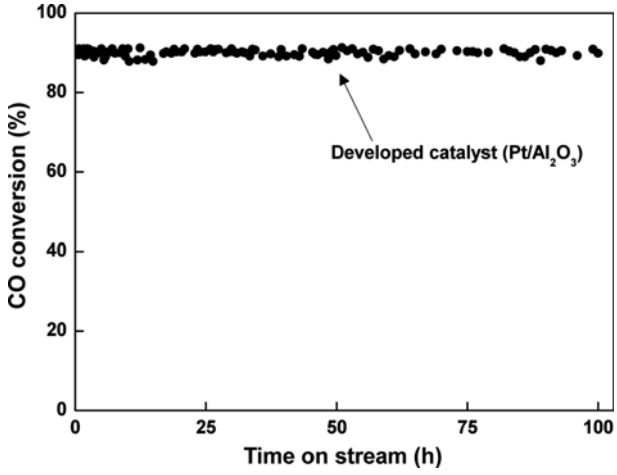

Fig. 6. CO conversion with time on stream over Pt/Al_2O_3 (Reaction condition: T=175 °C; $[O_2]/[CO]$=1.0; GHSV=46,129 h^{-1}).

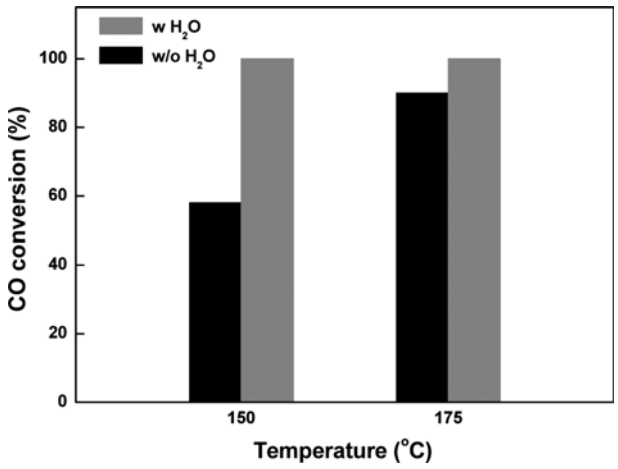

Fig. 7. Effect of H_2O addition on CO conversion over Pt/Al_2O_3 (Reaction condition: $H_2O/(CH_4+CO+CO_2)=1$; $[O_2]/[CO]=1.0$; GHSV=46,129 h^{-1}).

In real reforming processes, the PROX feed gas contains H_2O produced during WGS. Thus, the effect of H_2O addition on catalytic activity over Pt/Al_2O_3 catalyst is shown in Fig. 7. Due to the limitations of the reactor, the reaction containing H_2O could not be carried out below 150 °C. However, Pt/Al_2O_3 with H_2O had the 100% CO conversion at reaction temperatures from 150 to 175 °C. Several authors discussed the reasons for enhancement the CO oxidation rate in the presence of H_2O, namely, occurrence of the WGS reaction, modification of Pt^0 to PtO_x, and formation of oxidant hydroxyl groups on the catalyst surface [23]. Therefore, the prepared Pt/Al_2O_3 catalyst shows better catalytic performance in the real reforming processes containing H_2O.

CONCLUSIONS

PROX using typical reformate gas (without H_2O) has been carried out over the supported Pt catalysts. A Pt/Al_2O_3 catalyst exhibits the highest CO conversion and CO_2 selectivity. Moreover, the Pt/Al_2O_3 catalyst shows stable activity (X_{CO}>90% at 175 °C for 100 h). The remarkable performance of the Pt/Al_2O_3 catalyst is due to its having the highest Pt dispersion, easier reducibility of PtO_x, and easier electron transfer of metallic Pt. In addition, Pt/Al_2O_3 catalyst was also tested in realistic condition with both CO_2 and H_2O. It revealed that H_2O addition enhances PROX activity over Pt/Al_2O_3 catalyst. Therefore, Pt/Al_2O_3 catalyst can be a promising catalyst for PROX for proton exchange membrane fuel cells.

ACKNOWLEDGEMENTS

This research was supported by Basic Science Research Program through the National Research Foundation of Korea (NRF) funded by the Ministry of Science, ICT and Future Planning (2013R1A1A1A05007370).

REFERENCES

1. H. P. Chang, C. L. Chou, Y. S. Chen, T. I. Hou and B. J. Weng, *Int. J. Hydrogen Energy*, **32**, 316 (2007).
2. D.-W. Jeong, W.-J. Jang, J.-O. Shim, W.-B. Han, H.-S. Roh, U. H. Jung and W. L. Yoon, *Renew. Energy*, **65**,102 (2014).
3. D.-W. Jeong, H. S. Potdar, J.-O. Shim, W.-J. Jang and H.-S. Roh, *Int. J. Hydrogen Energy*, **38**, 4502 (2013).
4. D.-W. Jeong, V. Subramanian, J.-O. Shim, W.-J. Jang, Y.-C. Seo, H.-S. Roh, J. H. Gu and Y. T. Lim, *Catal. Lett.*, **143**, 438 (2013).
5. D.-W. Jeong, H. S. Potdar and H.-S. Roh, *Catal. Lett.*, **142**, 439 (2012).
6. H.-S. Roh, H. S. Potdar, K.-W. Jun, S. Y. Han and J.-W. Kim, *Catal. Lett.*, **93**, 203 (2004).
7. J. E. Park and E. D. Park, *Korean J. Chem. Eng.*, **31**, 1985 (2014).
8. A. Mishra and R. Prasad, *Bull. Chem. React. Eng. Catal.*, **6**, 1 (2011).
9. N. Mori, T. Nakamura, O. Sakai, Y. Iwamoto and T. Hattori, *Ind. Eng. Chem. Res.*, **47**, 1421 (2008).
10. E.-Y. Ko, E. D. Park, H. C. Lee, D. Lee and S. Kim, *Angew. Chem. Int. Ed.*, **46**, 734 (2007).
11. M. Kahlich, H. Gasteiger and R. Behm, *J. Catal.*, **182**, 430 (1999).
12. M. Bollinger and M. Vannice, *Appl. Catal. B: Environ.*, **8**, 417 (1996).
13. M. Shou, H. Takekawa, D.-Y. Ju, T. Hagiwara, D.-L. Lu and K.-I. Tanaka, *Catal. Lett.*, **108**, 119 (2006).
14. E. Gy. Szabó, A. Tompos, M. Hegedus, A. Szegedi and J. L. Margitfalvi, *Appl. Catal. A: Gen.*, **320**, 114 (2007).
15. H. Igarashi, H. Uchida, M. Suzuki, Y. Sasaki and M. Watanabe, *Appl. Catal. A: Gen.*, **159**, 159 (1997).
16. Y.-F. Han, M. J. Kahlich, M. Kinne and R. J. Behm, *Appl. Catal. B: Environ.*, **50**, 209 (2004).
17. H. Wakita, Y. Kani, K. Ukai, T. Tomizawa, T. Takeguchi and W. Ueda, *Appl. Catal. A: Gen.*, **283**, 53 (2005).
18. O. Pozdnyakova, D. Teschner, A. Wootsch, J. Kröhnert, B. Steinhauer, H. Sauer, L. Toth, F. C. Jentoft, A. Knop-Gericke, Z. Paál and R. Schlögl, *J. Catal.*, **237**, 1 (2006).
19. C. Pedrero, T. Waku and E. Iglesia, *J. Catal.*, **233**, 242 (2005).
20. C. Gu, S. Lu, J. Miao, Y. Liu and Y. Wang, *Int. J. Hydrogen Energy*, **35**, 6113 (2010).
21. F. Mariño, C. Descorme and D. Duprez, *Appl. Catal. B: Environ.*, **58**, 175 (2005).
22. Z. Wu, H. Zhu, Z. Qin, H. Wang, J. Ding, L. Huang and J. Wang, *Fuel*, **104**, 41 (2013).
23. V. Sebastian, S. Irusta, R. Mallada and J. Santamaría, *Appl. Catal. A: Gen.*, **366**, 242 (2009).
24. C. S. Polster, R. Zhang, M. T. Cyb, J. T. Miller and C. D. Baertsch, *J. Catal.*, **273**, 50 (2010).
25. L. Ilieva, T. Tabakova, G. Pantaleo, I. Ivanov, R. Zanella, D. Paneva, N. Velinov, J. W. Sobczak, W. Lisowski, G. Avdeev and A. M. Venezia, *Appl. Catal. A: Gen.*, **467**, 76 (2013).
26. F. Mariño, C. Descorme and D. Duprez, *Appl. Catal. B: Environ.*, **54**, 59 (2004).
27. Z. Yao, X. Zhang, F. Peng, H. Yu, H. Wang and J. Yang, *Int. J. Hydrogen Energy*, **36**, 1955 (2011).
28. M. M. Schubert, A. Venugopal, M. J. Kahlich, V. Plzak and R. J. Behm, *J. Catal.*, **222**, 32 (2004).
29. S. Malwadkar, P. Bera, M. S. Hegde and C. V. V. Satyanarayana, *Reac. Kinet. Mech. Cat.*, **107**, 405 (2012).
30. O. H. Laguna, M. I. Domínguez, S. Oraá, A. Navajas, G. Arzamendi, L. M. Gandía, M. A. Centeno, M. Montes and J. A. Odriozola, *Catal.*

Today, **203**, 182 (2013).
31. D. G. Oliva, J. A. Francesconi, M. C. Mussati and P. A. Aguirre, *J. Power Sources*, **182**, 307 (2008).
32. M. M. V. M. Souza, N. F. P. Ribeiro and M. Schmal, *Int. J. Hydrogen Energy*, **32**, 425 (2007).
33. N. An, X. Y. B. Pan, Q. Li, S. Li and W. Zhang, *RSC Adv.*, **4**, 38250 (2014).
34. D.-W. Jeong, A. Jha, W.-J. Jang, W.-B. Han and H.-S. Roh, *Chem. Eng. J.*, **265**, 100 (2015).
35. J. E. Park, B. B. Kim and E. D. Park, *Korean J. Chem. Eng.*, **32**, 2212 (2015).
36. G. Uysal, A. N. Akın, Z. İ. Önsan and R. Yıldırım, *Catal. Lett.*, **108**, 193 (2006).
37. Y. Hao, M. Mihaylov, E. Ivanova, K. Hadjiivanov, H. Knözinger and B. C. Gates, *J. Catal.*, **261**, 137 (2009).
38. E. G. Szabó, M. Hegedűs, F. Lónyi, Á. Szegedi, A. K. Datye and J. L. Margitfalvi, *Catal. Commun.*, **10**, 889 (2009).
39. A. Di Benedetto, G. Landi, L. Lisi and G. Russo, *Appl. Catal. B: Environ.*, **142-143**, 169 (2013).
40. D. Gamarra and A. Martínez-Arias, *J. Catal.*, **263**, 189 (2009).
41. H.-S. Roh, D.-W. Jeong, K.-S. Kim, I.-H. Eum, K. Y. Koo and W. L. Yoon, *Catal. Lett.*, **141**, 95 (2011).
42. D.-W. Jeong, W.-J. Jang, H.-S. Na, J.-O. Shim, A. Jha and H.-S. Roh, *J. Ind. Eng. Chem.*, **27**, 35 (2015).
43. D.-W. Jeong, W.-J. Jang, J.-O. Shim, W.-B. Han, H.-M. Kim, Y.-L. Lee, J. W. Bae and H.-S. Roh, *Renew. Energy*, **79**, 78 (2015).
44. D.-W. Jeong, H.-S. Na, J.-O. Shim, W.-J. Jang and H.-S. Roh, *Catal. Sci. Technol.*, **5**, 3706 (2015).
45. J. Shou-Yong, L. Li-Bin, H. Ning-Kang, Z. Jin and L. Yong, *J. Mater. Sci. Lett.*, **19**, 225 (2000).
46. K. Y. Koo, U. H. Jung and W. L. Yoon, *Int. J. Hydrogen Energy*, **39**, 5696 (2014).
47. P. Aunbamrung and A. Wongkaew, *Adv. Chem. Engineer. Sci.*, **3**, 15 (2013).
48. D. Widmann, Y. Liu, F. Schüth and R. J. Behm, *J. Catal.*, **276**, 292 (2010).
49. L. Delannoy, N. Weiher, N. Tsapatsaris, A. M. Beesley, L. Nchari, S. L. M. Schroeder and C. Louis, *Top. Catal.*, **44**, 263 (2007).
50. J. Z. Shyu and K. Otto, *Appl. Surf. Sci.*, **32**, 246 (1988).
51. K. Qadir, S. H. Kim, S. M. Kim, H. Ha and J. Y. Park, *J. Phys. Chem. C*, **116**, 24054 (2012).
52. T.-C. Chiu, H.-Y. Lee, P.-H. Li, J.-H. Chao and C.-H. Lin, *Nanotechnology*, **24**, 115601 (2013).
53. F.-C. Wang, C.-H. Liu, C.-W. Liu, J.-H. Chao and C.-H. Lin, *J. Phys. Chem. C*, **113**, 13832 (2009).
54. Y. Denkwitz, B. Schumacher, G. Kučerová and R. J. Behm, *J. Catal.*, **267**, 78 (2009).
55. Y. Zhang, S. Wu, L. Jin and D. Xie, *Int. J. Hydrogen Energy*, **39**, 18668 (2014).
56. L. E. Gómez, B. M. Sollier, M. D. Mizrahi, J. M. Ramallo López, E. E. Miró and A. V. Boix, *Int. J. Hydrogen Energy*, **39**, 3719 (2014).
57. P. Ratnasamy, D. Srinivas, C. V. V. Satyanarayana, P. Manikandan, R. S. Senthil Kumaran, M. Sachin and V. N. Shetti, *J. Catal.*, **221**, 455 (2004).
58. R. Padilla, M. Benito, L. Rodríguez, A. Serrano-Lotina and L. Daza, *J. Power Sources*, **192**, 114 (2009).
59. R. J. Baxter and P. Hu, *J. Chem. Phys.*, **116**, 4379 (2002).
60. Y. Huang, A. Wang, X. Wang and T. Zhang, *Int. J. Hydrogen Energy*, **32**, 3880 (2007).